Zinc-binding motif acts as an oxidative stress sensor to regulate TRPM7 channel activity

Hana Inoue[1#]*, Takashi Murayama[2#], Takuya Kobayashi[2], Masato Konishi[1], and Utako Yokoyama[1]*

[1]Department of Physiology, Tokyo Medical University, Tokyo, Japan

[2]Department of Cellular and Molecular Pharmacology, Juntendo University Graduate School of Medicine, Tokyo, Japan

# These authors contributed equally to this work.

Keywords: TRPM7, oxidative stress, zinc-binding motif, kinase domain

Abbreviated title: Oxidative stress sensor in TRPM7

(text 31 pages with 6 figures and 1 supplemental figure)

**Correspondence*: Hana Inoue, Department of Physiology, Tokyo Medical University, 6-1-1 Shinjuku, Shinjyuku-ku, Tokyo 160-8402, Japan. Tel: 81-3-3351-6141, Fax: +81-3-5379-0658, E-mail: hana@tokyo-med.ac.jp; Utako Yokoyama, Department of Physiology, Tokyo Medical University, 6-1-1 Shinjuku, Shinjyuku-ku, Tokyo 160-8402, Japan. Tel: 81-3-3351-6141, Fax: +81-3-5379-0658, E-mail: uyokoyam@tokyo-med.ac.jp

Abstract

TRPM7 channel activity is negatively regulated by intracellular Mg^{2+}. We previously reported that TRPM7 was inhibited by oxidative stress due to an enhancement of the inhibition by intracellular Mg^{2+}. In the present study, we aimed to clarify the precise mechanism underlying the TRPM7 inhibition by oxidative stress induced by hydrogen peroxide (H_2O_2). Site-directed mutagenesis on full-length TRPM7 revealed that none of the cysteines other than C1809 and C1813 within the zinc-binding motif of the TRPM7 kinase domain was involved in the H_2O_2-induced TRPM7 inhibition. When C1809 or C1813 was mutated, full-length TRPM7 failed to be expressed on the plasmamembrane. We therefore developed a novel approach in which the full-length TRPM7 is functionally reconstituted by co-expressing the TRPM7 channel domain (M7cd) and the TRPM7 kinase domain (M7kd) as separate individual proteins in HEK293 cells. When M7cd was expressed alone, the current was inhibited by intracellular Mg^{2+} stronger than in full-length TRPM7. Co-expression of M7cd and M7kd attenuated the current inhibition by intracellular Mg^{2+}, and the current was sensitive to oxidative stress, indicating a successful reconstitution of a full-length TRPM7-like current. A similar current reconstitution was observed when M7cd co-expressed with the kinase inactive mutant M7kd-K1645R. Thus, it was suggested that the kinase activity might not be essential for the reconstitution. Co-expression of M7cd and M7kd carrying a mutation at C1809 or C1813 failed to restore the full-length TRPM7-like current. No reconstitution was also observed with M7kd carrying a mutation at H1750 and H1807, which are involved in the zinc-binding motif formation together with C1809 and C1813. These data suggest that the zinc-binding motif is essential for the intracellular Mg^{2+}-dependent regulation of the TRPM7 channel activity by M7kd, and the cysteines in the

zinc-binding motif might play a role in the oxidative stress response of TRPM7.

Introduction

Magnesium ions are important for numerous cellular functions including cell cycles, channel regulation, enzyme activity, and energy metabolism (reviewed in (Wolf and Trapani, 2008; Romani, 2011; de Baaij et al., 2015). TRPM7 is an Mg^{2+}-permeable nonselective cation channel containing a serine/threonine protein kinase at its carboxyl terminus (Bates-Withers et al., 2011; Fleig and Chubanov, 2014). As the TRPM7 channel is activated upon the reduction of intracellular Mg^{2+} ($[Mg^{2+}]_i$) and thereby allows an Mg^{2+} influx, TRPM7 is considered to play a role in cellular Mg^{2+} homeostasis (Paravicini et al., 2012; Chubanov et al., 2018). It has been reported that TRPM7-deficient cells exhibit an impairment of proliferation and survival rate and that these defects are rescued by culturing in a medium containing high Mg^{2+} (Nadler et al., 2001; Schmitz et al., 2003; Schmitz et al., 2005; Chubanov et al., 2016). A global knockout of TRPM7 in mice results in early embryonic death (Jin et al., 2008; Liu et al., 2011; Jin et al., 2012). This lethality might result from the loss of TRPM7 channel activity but not loss of its kinase activity because kinase-inactive TRPM7 knock-in mice ($TRPM7^{K1646R/K1646R}$), in which TRPM7 current is comparable to that in wild-type mice, develop and live normally with no signs of Mg^{2+} deficiency throughout their lifespan (Kaitsuka et al., 2014). Thus, the channel activity of TRPM7 rather than its kinase activity is pivotal for Mg^{2+} homeostasis under basal conditions.

Although the kinase activity of TRPM7 is not essential for the channel activity (Schmitz et al., 2003; Matsushita et al., 2005; Demeuse et al., 2006; Inoue et al., 2014; Kaitsuka et al., 2014), the kinase domain might regulate the channel (Schmitz et al.,

2003; Desai et al., 2012; Yu et al., 2013). Whole deletion of the kinase domain (TRPM7-Δkinase) increases $[Mg^{2+}]_i$ sensitivity of the TRPM7 channel (Schmitz et al., 2003; Demeuse et al., 2006; Ryazanova et al., 2010), whereas the kinase inactive point mutant (K1645R) does not affect its $[Mg^{2+}]_i$ sensitivity (Matsushita et al., 2005). Consistently, reduction of TRPM7 current and defect in Mg^{2+} homeostasis are observed in $TRPM7^{+/\Delta kinase}$ but not in $TRPM7^{K1646R/K1646R}$ mice (Ryazanova et al., 2010; Kaitsuka et al., 2014; Romagnani et al., 2017). Thus, it is plausible that the structural interactions between the channel domain and the kinase domain are important for the $[Mg^{2+}]_i$-mediated regulation of TRPM7 channel activity.

We have previously reported that oxidative stress induced by hydrogen peroxide (H_2O_2) inhibits TRPM7 channel activity by sensitizing the channel to $[Mg^{2+}]_i$ (Inoue et al., 2014). Our previous study demonstrated that the cysteine modulator N-methyl maleimide (NMM) inhibited the TRPM7 current in a similar Mg^{2+}-dependent fashion to H_2O_2, suggesting that cysteines might act as an oxidative sensor. However, precise molecular mechanisms underlying the oxidative stress-induced TRPM7 inhibition remain to be clarified. In this study, we tried to identify the oxidative stress sensors targeted by H_2O_2 in TRPM7. Our data suggested that the zinc-binding motif of the TRPM7 kinase domain is responsible for the interaction between the channel domain and the kinase domain to regulate $[Mg^{2+}]_i$ sensitivity and that the oxidation of cysteines in the zinc-binding motif under oxidative stress might interfere with the interaction to inhibit the TRPM7 current.

Materials and methods

Vector constructions

Amino-terminal streptavidin binding peptide (SBP)-tagged full-length wild-type mouse TRPM7 (SBP-mTRPM7-wt) expression vectors were prepared by inserting nucleotides encoding a SBP tag (MDEKTTGWRGGHVVEGLAGELEQLRARLEHHPQGQREP) after the first methionine into an mTRPM7-wt pcDNA5/FRT/TO vector generated previously (Inoue et al., 2014). A full-length cDNA of human TRPM7 (hTRPM7) (pF1KE3491) was purchased from Kazusa Genome Technologies (Chiba, Japan). The hTRPM7 was cloned into a doxycycline-inducible expression vector pcDNA/FRT/TO (Invitrogen, Carlsbad, CA, USA), and the nucleotides encoding the SBP tag were inserted after the first methionine. Mouse TRPM7 channel domain (M7cd, a.a. 1-1509) was prepared by inserting a stop codon and *XhoI* site after 1509 by PCR using a *BstXI-SalI* fragment as the PCR template. The TRPM7 kinase domain (M7kd; a.a.1511-1863) was amplified by PCR using an mTRPM7-wt pcDNA5/FRT/TO vector as the template with the primers 5'-CC*ACGCGT*GCCACC<u>ATG</u>TCTAAAGCAGCTTTGTTACC-3' (Mlu□ site in italics) including the ATG start codon (underlined) and 5'-CC*CTCGAG*CTATAACATCAGACGAACAG-3' (Xho□ site in italics). The PCR product was cloned into a pIRES2-EGFP expression vector (BD Biosciences Clontech Franklin Lakes, NJ, USA) in which the Mlu□ site was inserted at the multi cloning site using the Mlu□ and Xho□ sites. The full-length coding sequence of mouse TRPM6 (AY333282) was amplified by PCR using cDNA of mouse kidney at the template with the primers 5'-CC*GTCGAC*ATGCAGGTCAAGAAATCCTG-3' (Sal□ site in italics) and 5'-CC*GGATCC*TTAAAGGCGTGTGTGATCTT-3' (M6 reverse primer; BamH□

site in italics) and cloned into pBluescript SK(-) (Stratagene, La Jolla, CA, USA), using the Sal□ and BamH□ sites. The TRPM6 kinase domain (M6kd; a.a.1651-2028) was amplified by PCR using mTRPM6-wt pBluescript SK(-) vector as the template with the forward primer 5'-CC*ACGCGT*GCCACCATGAAAATGAAGGAAATCAAG-3' (Mlu□ site in italics) including the ATG start codon (underlined) and the M6 reverse primer, and cloned into the pIRES2-EGFP expression vector, using the Mlu□ and BamH□ sites. Amino acid substitution mutants were generated by site-directed mutagenesis using a QuickChange site-directed mutagenesis kit (Agilent Technologies, La Jolla, CA, USA). The predicted DNA sequences of all constructs were verified by sequencing.

Baculovirus production

Baculovirus carrying vesicular stomatitis VSVG (virus G protein) on the virus envelope that effectively infects mammalian cells was produced as described previously (Uehara et al., 2017). cDNAs for wild-type and mutant M7kd were cloned into the modified pFastBac1 vector (Invitrogen) using the MluI and XhoI sites. Baculovirus was produced in Sf9 cells according to the manufacturer's instructions. A P2 virus was used for the experiments.

Cells

Stable and doxycycline-inducible HEK293 cell lines overexpressing wild-type, mutant, or the channel domain of mTRPM7 were generated as previously described (Inoue et al., 2014) using the Flp-In T-REx system (Invitrogen). Cells were maintained in a growth

medium, consisting of DMEM supplemented with 10% FBS, 2 mM Glutamax (Invitrogen), 100 μM hygromycin, 15 μM blasticidin, and penicillin-streptomycin (Invitrogen). To induce protein expression, doxycycline (1 μg/ml) was added to the culture medium the day before the experiments. Experiments were performed 16-30 h post-induction.

Transient expression of M7kd

HEK293 cells stably transfected with SBP tagged or non-tagged mM7cd were plated into a Φ35 mm dish (1×10^6 cell /dish) and cultured in the growth medium for 24 h. M7kd or its mutants encoded in pIRES2-EGFP vectors (2.5 μg/dish) were transfected using lipofectamine 3000 (Invitrogen) following the manufacturer's instructions. After an overnight incubation, cells were re-plated on glass cover slips coated with Matrigel (Corning, Corning, NY, USA) and cultured in the growth medium containing doxycycline (1 μg/ml) for 16-30 h.

For baculovirus-mediate expression, HEK293 cells stably expressing M7cd were plated into a 12-well plate (1.2×10^5 cell / well). The cells were cultured for 15-24 h in 900 μl of the growth medium containing doxycycline (1 μg/ml) and 100 μl of baculovirus P2 virus solutions.

HEK293 cells expressing M7kd were identified by EGFP fluorescence under an epifluorescence microscope.

Immunoblotting

Immunoblotting was performed as previously described (Inoue et al., 2014). Proteins in

the HEK293 cell lysates were separated by SDS-PAGE using 3-15% linear gradient gels and electrophoretically transferred onto PVDF membranes. To detect full-length TRPM7, its mutants, and M7cd, rabbit anti-TRPM7 antibody (ACC-047; epitope 1146-1165 of human TRPM7, Alomone Labs, Jerusalem, Israel) was used. Rabbit anti-TRPM7+TRPM6 antibody (ab109438; epitope 1800-C-terminus of human TRPM7, Abcam Biochemicals, Bristol, UK) were used to detect M7kd.

Immunocytochemistry

Stable HEK 293 cells were plated on glass coverslips (Φ 13 mm) coated with Matrigel, and protein expression was induced by doxycycline (1 μg/ml) for 24 h. Cells were fixed in 4% formaldehyde for 10 min at RT, washed three times with PBS, and permeabilized in 0.2% Triton X-100 (Sigma-Aldrich, St. Louis, MO) in PBS for 10 min at RT. Cells were washed three times with cold PBS and incubated with 1% bovine serum albumin (BSA) in PBS for 10 min and then with goat anti-TRPM7 antibody (ab729; Abcam Biochemicals) for 16 h at 4°C. After three washes with 1% BSA-PBS, cells were incubated with a secondary antibody, FITC-conjugated donkey anti goat IgG (ab6881; Abcam). After three washes with 1% BSA-PBS, coverslips were mounted for confocal microscopic imaging (Fluoview ver. 10; Olympus, Tokyo, Japan).

Patch-clamp experiments

All experiments were conducted at room temperature (23-25°C). The patch electrodes were prepared from borosilicate glass capillaries and had a resistance of 1.5-2.2 MΩ when filled with a pipette solution (see below). Series resistance (< 3 MΩ) was

compensated (80%) to minimize voltage errors. Currents were recorded using an Axopatch 200B amplifier (Molecular Devices, Union City, CA, USA) coupled to a DigiData 1550 A/D and D/A converter (Molecular Devices). Current signals were filtered at 1 kHz using a four-pole Bessel filter and were digitized at 5 kHz. pClamp 10.6 software was used for the command pulse protocol, data acquisition, and analysis. The time courses of the current were monitored by repetitively applying (every 10 s) a ramp pulse from -100 to +100 mV (1-s duration) from a holding potential of 0 mV. The control bath solution consisted of (mM): 135 NaCl, 5 KCl, 1 $MgCl_2$, 1 $CaCl_2$, 1.2 NaH_2PO_4, 10 HEPES, 2 glucose, and 27 mannitol (pH 7.4 adjusted with NaOH, 315 mOsmol/kgH_2O). The intracellular (pipette) solutions were as follows (mM): 25 CsCl, 110 CsOH, 110 glutamate, 0.2 EGTA, 10 EDTA, and 5 HEPES (pH 7.3 adjusted with CsOH, 290 mOsmol/kgH_2O). $MgSO_4$ was added to vary the free Mg^{2+} concentration ([Mg^{2+}]). For the intracellular solution containing 20.9 μM or 0.2 mM [Mg^{2+}], EDTA was replaced with HEDTA. For the intracellular solution containing [Mg^{2+}] higher than 0.5 mM, EDTA was eliminated. [Mg^{2+}] was calculated using MaxChelator software (https://somapp.ucdmc.ucdavis.edu/pharmacology/bers/maxchelator/webmaxc/webmaxcS.htm). H_2O_2 or NMM was applied to the extracellular solution for 4 min, and the current amplitudes were analyzed at the end of the application. The current amplitudes just before the application of H_2O_2 or NMM were considered to represent the control.

Statistical analysis

Data are given as means ± SEM of observations. Comparisons of two experimental groups were made using Student's *t*-test. Data were considered to be significant at $P < 0.05$.

For the analysis of concentration-dependent inhibition, data were fitted with a monophasic concentration-response curve provided by the Origin software fitting subroutine (OriginLab, Northampton, MA, USA). The formula for monophasic concentration-response curves is as follows:

$$y = \text{Bottom} + \frac{\text{Top} - \text{Bottom}}{1 + 10^{(\log \text{IC50} - x)\text{slope}}}$$

where Bottom and Top are the plateaus at the left and right ends of the curve. IC_{50} is a concentration that gives a half-maximal inhibitory effect.

Results

Mouse TRPM7 and human TRPM7 were inhibited by H_2O_2 in a $[Mg^{2+}]_i$-dependent manner

It is well established that TRPM7 channel activity is inhibited by intracellular Mg^{2+}. We previously reported that oxidative stress induced by H_2O_2 inhibited both overexpressed mouse TRPM7 (mTRPM7) current in HEK293 cells (Inoue et al., 2014), as well as endogenous TRPM7 current in mouse white adipocytes (Inoue et al., 2019). Whole-cell recordings revealed that spontaneous current activation comparable to that of the previous study was observed after an establishment of whole-cell configuration (break-in) in mTRPM7-wt expressing HEK293 cells, probably due to reduction of intracellular free concentration of Mg^{2+} ($[Mg^{2+}]_i$) from ~0.9 mM presumed in cytosol to 0.2 mM in the pipette solution (Figure 1A). The activated current was markedly inhibited by an application of H_2O_2 (500 μM) (250.9 ± 21.8 pA/pF and 73.4 ± 12.7 pA/pF at +80 mV, before and 4 min after application of H_2O_2, respectively, n = 10) (Figure 1A). Although the spontaneous activation was less obvious in the presence of

physiological $[Mg^{2+}]_i$ (1 mM), H_2O_2 still inhibited the current significantly (120.3 ± 17.4 pA/pF and 58.8 ± 12.8 pA/pF at +80 mV, before and 4 min after application of H_2O_2, n = 10, respectively) (Figure 1B). TRPM7 current is inhibited by intracellular free Mg^{2+} in a dose-dependent manner with an IC_{50} of 427 μM in the presence of extracellular divalent cations, and H_2O_2 shifted the $[Mg^{2+}]_i$-dependent inhibition curves to 100-fold lower concentrations with an IC_{50} of 4.3 μM (Figure 1C). It has been reported that mTRPM7-S1107E mutant is insensitive to $[Mg^{2+}]_i$ (Hofmann et al., 2014; Zhelay et al., 2018). Consistently, the spontaneous current activation after break-in was not observed in mTRPM7-S1107E mutant in whole-cell recordings (Figure 1D). An application of H_2O_2 (500 μM) did not affect mTRPM7-S1107E current even in the presence of higher $[Mg^{2+}]_i$ (Figure 1E and F). These data support the concept that H_2O_2-induced inhibition is due to an enhancement of Mg^{2+}-inhibition.

Furthermore, it was confirmed that human TRPM7 current was inhibited by H_2O_2 (500 μM) or NMM (100 μM) in a similar $[Mg^{2+}]_i$-dependent fashion (Supplemental Figure). These data indicated that mouse and human TRPM7 are similarly regulated by oxidative stress.

Cleavage of TRPM7 by caspases was not involved in H_2O_2-induced TRPM7 inactivation

It has been reported that TRPM7 is cleaved by caspases at position D1510, and the released TRPM7 kinase domain translocates to the nucleus (Desai et al., 2012) (Krapivinsky et al., 2014). The truncated TRPM7 channel domain can be expressed on the plasma membrane (Desai et al., 2012; Duan et al., 2018), though the channel activity is strongly inhibited by intracellular Mg^{2+} (Schmitz et al., 2003). Since H_2O_2 activates caspases, it might be possible that caspases mediate the inhibition of TRPM7

by cleaving the kinase domain from TRPM7. To test this possibility, another HEK293 cell line that expressed a caspase cleavage resistant mutant, TRPM7-D1510A, was established (Figure 1G). Similar to TRPM7-wt (Figure 1A), TRPM7-D1510A was markedly inhibited by H_2O_2. These data suggested that caspase-mediated cleavage of TRPM7 was not involved in the current inhibition that occurred at least during short (4-min) exposure to H_2O_2.

Screening of cysteines involved in H_2O_2-induced TRPM7 inactivation

Since cysteine is one of the most vulnerable amino acid residues to oxidative stress in proteins, it might be possible that H_2O_2 oxidizes cysteine(s) in TRPM7 and thereby induces $[Mg^{2+}]_i$-dependent inactivation of the channel activity. Consistent with our previous reports, N-methyl maleimide (NMM) (100 μM), a cysteine-modulating reagent, inhibited mTRPM7 in a similar fashion to H_2O_2 (Figure 1H and I). We then screened for 34 cysteines that are conserved both in mouse and human TRPM7 (Figure 2A) by employing site-directed mutagenesis to identify the oxidation targets during exposure to H_2O_2. HEK293 cell lines that stably express each mutant by doxycycline treatment were established. The protein expression of each mutant, including a mutant lacking 55 N-terminus amino acids that contained 7 cysteines (ΔNt7C) as well as single- or double-point mutants of cysteine (C) replaced with alanine (A), was confirmed by Western blotting in doxycycline-treated (Dox [+]) HEK 293 cells (Figure 2B). All alanine mutants, except those at the positions C721, C738, C1809, and C1813, expressed robust currents distinguishable from endogenous currents in doxycycline-untreated (Dox [-]) HEK293 cells in the presence of 0.2 mM $[Mg^{2+}]_i$ (Figure 2C). The current amplitudes in the control conditions were varied among

mutants, yet H_2O_2 consistently decreased the currents to ~30% of those before H_2O_2 treatment in each mutant, suggesting that these cysteines are not the target for the oxidation by H_2O_2 to inhibit the current (Figure 2C). Although the protein expression of TRPM7-C721A, -C738A, -C1809A, and -C1813A were detected in whole-cell lysates by Western blotting (Figure 2B), the current amplitude in these mutants was indistinguishable from that in Dox [-]-cells (Figure 2C).

Immunocytochemistry revealed that mTRPM7-wt was clearly detected at the cell boundaries, suggesting the expression on the plasma membrane (Figure 3). Consistent with the electrophysiology results, TRPM7-C721A and -C738A seemed to be retained in the intracellular compartments but not expressed on the plasma membrane (Figure 3). Instead of alanine mutants, serine mutants of C721 and C738 could be expressed on the plasma membrane (Figure 3) and exhibit a robust current that was sensitive to H_2O_2 (Figure 2C). On the other hand, a serine mutant of C1809 and C1813, both located in the zinc-binding motif at the C-terminus and important for structural integrity of TRPM7 kinase domain (Runnels et al., 2001) (Yamaguchi et al., 2001), still failed to be expressed on the plasma membrane (Figure 3).

M7cd was functionally expressed in HEK293 cells

Since the cysteine mutations in the zinc-binding motif of TRPM7 interfered with the membrane expression, we developed a novel approach in which the full-length TRPM7 was functionally reconstituted by co-expressing M7cd and M7kd as separate proteins in a cell.

We established a HEK293 cell line that stably expresses M7cd (a.a. 1-1510). Whole-cell recordings confirmed that doxycycline treatment induced functional

expression of M7cd on the plasma membrane in the absence of intracellular Mg^{2+} (Figure 4A). Consistent with the previous report demonstrating that TRPM7-Δkinase (deletion after a.a. 1569) is strongly inhibited by intracellular Mg^{2+} (Schmitz et al., 2003), M7cd current was much smaller compared to the full-length TRPM7-wt current in the presence of 0.2 mM $[Mg^{2+}]_i$ (243.7 ± 22.6 pA/pF and 28.4 ± 4.4 pF/pA at +80 mV at 2 min after break-in, in full-length TRPM7-wt and M7cd, n = 10 and 21, respectively) (Figure 1A and 4B). It was revealed that M7cd current was inhibited by intracellular Mg^{2+} with an IC_{50} of 5.6 μM (Figure 4F). On the other hand, M7cd carrying a S1107E mutation (M7cd-S1107E) expressed robust currents constantly in the absence or presence of 0.2 mM $[Mg^{2+}]_i$ (192.5 ± 18.3 pA/pF and 217.9 ± 26.9 pF/pA at +80 mV at 2 min after break-in, in the absence or presence of 0.2 mM $[Mg^{2+}]_i$, n = 10 and 7, respectively) (Figure 4C). These results suggested that M7kd attenuates the Mg^{2+}-dependent inhibition of M7cd.

Functional reconstitution of TRPM7 by co-expression of M7cd and M7kd

To test the effect of the co-expression of M7kd on the M7cd current, M7kd (a.a. 1511-1863) was separately expressed in M7cd-expressing HEK293 cells. In M7cd and M7kd co-expressing cells, the spontaneous current activation after break-in was observed in the presence of 0.2 mM $[Mg^{2+}]_i$ similarly to full-length TRPM7-wt (Figure 4D). H_2O_2 (500 μM) significantly inhibited the reconstituted current in the presence of 0.2 mM $[Mg^{2+}]_i$ (565.7 ± 68.9 pA/pF and 14.0 ± 3.2 pA/pF at +80 mV, before and 4 min after application of H_2O_2, n = 8, respectively), but not in the absence of Mg^{2+} (1226.1 ± 240.2 pA/pF and 852.5 ± 184.9 pA/pF at +80 mV, before and 4 min after application of H_2O_2, n = 8, respectively) (Figure 4D and E). The Mg^{2+}-dependent curve of M7cd

current was shifted rightward by the co-expression of M7kd from an IC_{50} of 5.6 μM in the absence of M7kd to 349 μM, which is comparable to that of full-length TRPM7-wt (Figure 4F). M7kd attenuates $[Mg^{2+}]_i$-dependent inhibition regardless of whether it is tethered to M7cd.

During whole-cell recordings in M7cd-expressing HEK293 cells transfected with M7kd-expression vector by lipofection, the current was sometimes declined after the spontaneous activation before an application of H_2O_2 (Figure 4D and G). Since M7kd was expressed as a cytosolic mobile protein rather than as a plasma membrane-anchored protein, it could be easily diluted with the pipette solutions during whole-cell recordings. Thus, the decline of the current might result from a decrease in M7kd after break-in. Consistently, when M7kd was expressed with a baculovirus vector that was supposed to enable the highly efficient expression of M7kd, the current was maintained at least during 6-min recordings (Figure 4G). It was suggested that the amount of M7kd was sufficient even after the dilution with the pipette solution when M7kd was expressed with a baculovirus vector. H_2O_2 (500 μM) inhibited the reconstituted current in HEK293 cells co-expressing M7cd and M7kd by baculovirus transfection. Therefore, transfection of M7kd with either lipofection or the baculovirus could reconstitute a comparable full-length TRPM7 (Figure 4H and I).

Kinase activity was not involved in the M7kd-mediated regulation of $[Mg^{2+}]_i$-dependent regulation of M7cd

We previously reported that a full-length, kinase-inactive point mutant TRPM7-K1645R is inhibited by H_2O_2 similarly to TRPM7-wt (Inoue et al., 2014). Co-expression of M7kd-K1645R in M7cd-expressing cells also generated a substantial current that was

inhibited by H_2O_2 (500 μM) (Figure 4J), indicating reconstitution of the full-length TRPM7-K1645R. It was suggested that the kinase activity is not essential to relieve M7cd from $[Mg^{2+}]_i$-dependent inhibition. Consistent results were obtained when M7cd was co-expressed with a kinase domain of TRPM6 (M6kd), which is the closest homologue of TRPM7, but their kinase functions are not redundant (Schmitz et al., 2005) (Figure 4K). M6kd (a.a. 1650-2028) could also attenuate $[Mg^{2+}]_i$-dependent inhibition of M7cd, possibly because of their structural similarity since both kinases contain a zinc-binding motif at the C-terminus. Co-expression of M7cd and M6kd reconstituted a full-length TRPM7-like current that is inhibited by H_2O_2 (500 μM) (Figure 4K).

Mutations of cysteines in the zinc-binding motif interfered with the functional interaction between M7cd and M7kd, which attenuates Mg^{2+}-dependent inhibition of TRPM7 current

To examine the effect of mutations of C1809 and C1813, M7kd-C1809S or -C1813S was expressed in M7cd-expressing HEK293 cells. The protein expression of M7cd and M7kd was confirmed by Western blotting by using different antibodies targeting M7cd (ACC-047) and M7kd (ab109438) (Figure 5A). M7kd-wild type (wt) and the mutants, M7kd-C1809S and -C1813S, were expressed in HEK293 cells stably expressing M7cd.

In these settings, attenuation of the $[Mg^{2+}]_i$-dependent inhibition was not observed in M7cd and M7kd-C1809S or -C1813S co-expressing cells (Figure 5B, C, G). Co-expression of M7kd-C1809S did not affect M7cd-S1107E (Mg^{2+} insensitive mutant) current either before or after an application of H_2O_2 (500 μM) (Figure 5D), suggesting that the mutation of C1809 in M7kd does not have a direct inhibitory effect on the current *per se*.

The crystal structure of TRPM7 kinase domain (a.a. 1521-1863) reveals that a zinc atom is coordinated by H1750, H1807, C1809, and C1813 (Yamaguchi et al., 2001). Therefore, in addition to C1809 and C1813, we examined the involvement of H1750 and H1807 in the $[Mg^{2+}]_i$-dependent regulation of the M7cd current (Figure 5E, F, G). Co-expression of M7kd-H1750A or -H1807A indeed failed to reconstitute the full-length TRPM7-wt, indicating that the structural integrity of M7kd supported by the zinc-binding motif is important for attenuating the $[Mg^{2+}]_i$-dependent inhibition of M7cd.

Thus, it is indicated that the zinc-binding motif plays a key role in the functional interaction between M7cd and M7kd in attenuating the $[Mg^{2+}]_i$-dependent inhibition of the TRPM7 channel activity. Our data suggest that the oxidation of C1809 or C1813 by H_2O_2 disrupts the functional interaction between M7cd and M7kd to enhance the $[Mg^{2+}]_i$-dependent inhibition of the TRPM7 channel.

Discussion

In the present study, we found novel mechanisms underlying the regulation of TRPM7 channel activity by its kinase domain (Figure 6). It was revealed that intramolecular interactions between the channel domain and the kinase domain, but not phosphate transfers, increases TRPM7 current by attenuating TRPM7 inhibition by $[Mg^{2+}]_i$. Mutations of the cysteines, C1809 or C1813, in the zinc-binding motif that are important for the structural integrity of the TRPM7 kinase domain diminished the effects of the kinase domain on the TRPM7 current. Our data suggested that oxidative stress inhibits TRPM7 probably via oxidation of C1809 and/or C1813. Oxidation of these cysteines might disrupt the proper structure of the kinase domain and interfere

with the interaction between the channel domain and the kinase domain to enhance the inhibition of TRPM7 by intracellular Mg^{2+}.

Oxidation of cysteines and methionines in proteins regulates numerous redox-sensitive physiological functions (Rhee et al., 2000; Poole and Nelson, 2008; Reddie and Carroll, 2008; Klomsiri et al., 2011). Among TRPM family members, TRPM2 and TRPM6 have been reported to be regulated by oxidative stress via direct oxidation of a certain methionine residue (Cao et al., 2010; Kashio et al., 2012). Our present study suggested that C1809 and C1813 act as an oxidative stress sensor in TRPM7. The crystal structure of the TRPM7 kinase domain has revealed that these cysteines coordinate a zinc ion with H1750 and H1807 (Yamaguchi et al., 2001). This zinc-binding motif is important for the structural integrity of the TRPM7 kinase domain, and thus mutation of C1809 and C1813 results in a loss of kinase activity (Runnels et al., 2001). Since the kinase-inactive M7kd-K1645R as well as M6kd, which is a functionally non-redundant kinase to M7kd (Schmitz et al., 2005), attenuated the $[Mg^{2+}]_i$-dependent inhibition of M7cd current comparable to that of M7kd-wt (Figure 4J, K), this suggests that the kinase activity was not involved in the regulation of $[Mg^{2+}]_i$ sensitivity. On the other hand, M7kd-C1809 or -C1813 failed to increase the M7cd current (Figure 5B, C, G). Furthermore, our experiments showed that M7kd-H1750A or -H1807A also failed to attenuate the $[Mg^{2+}]_i$-dependent inhibition of the M7cd current (Figure 5E, F, G). From these results, it was suggested that the structural integrity of M7kd guaranteed by the zinc-binding motif is important for the interaction between M7cd and M7kd to regulate the $[Mg^{2+}]_i$-sensitivity of TRPM7. It has been proposed that the zinc-binding motif acts as an oxidative stress sensor in various proteins to regulate cellular functions in response to redox changes (Ilbert et al., 2006; Kroncke and Klotz, 2009). Likewise, the

zinc-binding motif of TRPM7 might be an oxidative sensor that regulates the channel activity.

In our electrophysiological experiments, EDTA or HEDTA was included in the pipette solutions to maintain constant $[Mg^{2+}]_i$, even in the presence of extracellular Mg^{2+}, when the $[Mg^{2+}]_i$ was set at < 0.5 mM (Materials and Methods). Besides Mg^{2+}, these chelators bind Zn^{2+} with a dissociation constant (K_d) of 2.3×10^{-14} or 6.6×10^{-13}, respectively (Krezel and Maret, 2016). Therefore, the use of these chelators might unfold the zinc-binding motif of TRPM7 by depleting a zinc ion under the whole-cell configuration. However, we were able to measure a robust TRPM7 current in the presence of the chelators (Figure 1), suggesting that the zinc-binding motif of TRPM7 provides a high-affinity binding site for zinc. It has been reported that a well-packed hydrophobic core in the vicinity of a zinc-binding motif increases the binding constant (K_a) to 10^{13}-10^{16} and slows down the kinetics of metal exchange using zinc finger peptide models (Seneque and Latour, 2010). In the zinc-binding motif of TRPM7, the zinc is integrated into the hydrophobic core and is secluded from solvent (Yamaguchi et al., 2001). Thus, the zinc-binding motif of TRPM7 might be folded as intact, even in the presence of the chelators, until H_2O_2 is applied.

Our results demonstrated that M7cd and M7kd interact functionally, but the interaction sites of M7cd with M7kd remain to be identified. Although the protein-protein interaction between M7cd and M7kd was tested using an immunoprecipitation technique in our preliminary experiments, M7kd was not co-immunoprecipitated with M7cd probably due to the low affinity between M7cd and M7kd. Consistently, electrophysiology data also suggested the weak binding of M7cd and M7kd (Figure 4G). When M7kd was overexpressed in M7cd-expressing cells as a separated individual

protein, the current was robust for several minutes after break-in, yet declined over time (Figure 4G). This might be due to a decrease in M7kd concentration in the cytosol through intracellular perfusion with the pipette solution. In a full-length TRPM7 in which M7cd and M7kd are tethered in a single molecule, the interaction might possibly attenuate the $[Mg^{2+}]_i$-dependent inhibition of the TRPM7 current. Thus, because of the weak binding of M7cd and M7kd, it is difficult to identify the interaction sites via a general immunoprecipitation technique or pull-down assay. Rather, structural analysis might be effective for clarifying the mechanism underlying the interaction. So far, the structure of the TRPM7 channel domain (lacking the kinase domain) and that of the TRPM7 kinase domain (lacking the channel domain) have been resolved independently (Yamaguchi et al., 2001; Duan et al., 2018). However, the whole structure of TRPM7 remains to be identified. Thus, further structural study might be necessary for identifying the interaction sites between M7cd and M7kd that regulate the channel activity.

Mutation of cysteines in the zinc-binding motif, as well as the alanine mutants of C721 and C738 in full-length TRPM7 failed to express on the plasmamembrane, and instead remained at an intracellular compartment (Figure 3). These results suggest that these cysteines might be important for the proper folding of TRPM7 to be expressed on the plasmamembrane. Heterozygous mutation of C721 to glycine in TRPM7 has been found in a human pedigree with macrothrombocytopenia (Stritt et al., 2016). In contrast to TRPM7-C721A, which was examined in the present study, the TRPM7-C721G mutant is successfully expressed on the plasmamembrane though the current is reduced by 85% of that of TRPM7-wt when expressed in HEK293 cells. The serine mutant of C721 (TRPM7-C721S) could be expressed on the plasmamembrane (Figure 3), and the

current was comparable to that of TRPM7-wt (Figure 2C). Thus, the results vary based on which amino acid is substituted for C721. The structure defined by C721 might be important not only for expression on the plasmamembrane but also for TRPM7 channel activity, but may not be involved in the oxidative stress-induced inhibition of TRPM7.

There has been growing interest in investigating the involvement of TRPM7 channel activity in a range of pathologies, such as ischemia in brain (Aarts et al., 2003; Sun et al., 2009; Chen et al., 2015a) and kidney (Meng et al., 2014; Liu and Yang, 2019), as well as cancer (Guilbert et al., 2009; Rybarczyk et al., 2012; Chen et al., 2015b; Liu et al., 2020). Downregulation of TRPM7 by small interference RNA or TRPM7 inhibitors alleviates ischemic damage in neurons (Chen et al., 2015a; Sun, 2017). Since TRPM7 is permeable for divalent cations including Ca^{2+} and Zn^{2+}, it is conceivable that the downregulation of TRPM7 protect cells from Ca^{2+}- or Zn^{2+}-induced toxicity associated with ischemia (Inoue et al., 2010; Sun, 2017). In cancer cells, it has been reported that increased activity of TRPM7 might be involved in cancer cell proliferation and migration (Guilbert et al., 2009; Rybarczyk et al., 2012; Chen et al., 2015b). Thus, downregulation of TRPM7 might be a therapeutic target under these pathological conditions. There are several potent inhibitors of TRPM7, such as waixenecin A (Zierler et al., 2011) and NS8593 (Chubanov et al., 2012), but the binding site of these compounds in the TRPM7 molecule remains largely unknown. Both waixenecin A and NS8593 inhibit TRPM7 current in the absence of intracellular Mg^{2+} or its kinase domain, but the inhibitory mechanisms are different from those of oxidative stress. Based on our present findings, compounds designed to interrupt the intramolecular interaction between M7cd and M7kd can be specific inhibitors for TRPM7.

In conclusion, oxidative stress inhibits TRPM7 channel activity. Cysteine residues of

the zinc-binding motif are suggested to act as the oxidative stress sensor, whose oxidation might interfere with the intramolecular interactions between the channel domain and the kinase domain, thereby increasing Mg^{2+}-dependent inhibition of the channel activity.

Disclosures

No conflicts of interest are declared by the authors.

Author contributions

H. Inoue carried out electrophysiological experiments and cell biological experiments. T. Murayama provided experimental tools and carried out biochemical experiments. T. Kobayashi provided experimental tools and useful discussions. H. Inoue and T. Murayama analyzed the data. H. Inoue, T. Murayama, M. Konishi, and U. Yokoyama wrote the manuscript. All authors discussed the results and approved the final version of the manuscript.

References

Aarts, M., K. Iihara, W.L. Wei, Z.G. Xiong, M. Arundine, W. Cerwinski, J.F. MacDonald, and M. Tymianski. 2003. A key role for TRPM7 channels in anoxic neuronal death. *Cell*. 115:863-877.

Bates-Withers, C., R. Sah, and D.E. Clapham. 2011. TRPM7, the Mg(2+) inhibited channel and kinase. *Adv Exp Med Biol*. 704:173-183.

Cao, G., K.P. Lee, J. van der Wijst, M. de Graaf, A. van der Kemp, R.J. Bindels, and J.G. Hoenderop. 2010. Methionine sulfoxide reductase B1 (MsrB1) recovers TRPM6 channel activity during oxidative stress. *J Biol Chem*. 285:26081-26087.

Chen, W., B. Xu, A. Xiao, L. Liu, X. Fang, R. Liu, E. Turlova, A. Barszczyk, X. Zhong, C.L. Sun, L.R. Britto, Z.P. Feng, and H.S. Sun. 2015a. TRPM7 inhibitor carvacrol protects

brain from neonatal hypoxic-ischemic injury. *Mol Brain*. 8:11.

Chen, W.L., A. Barszczyk, E. Turlova, M. Deurloo, B. Liu, B.B. Yang, J.T. Rutka, Z.P. Feng, and H.S. Sun. 2015b. Inhibition of TRPM7 by carvacrol suppresses glioblastoma cell proliferation, migration and invasion. *Oncotarget*. 6:16321-16340.

Chubanov, V., S. Ferioli, A. Wisnowsky, D.G. Simmons, C. Leitzinger, C. Einer, W. Jonas, Y. Shymkiv, H. Bartsch, A. Braun, B. Akdogan, L. Mittermeier, L. Sytik, F. Torben, V. Jurinovic, E.P. van der Vorst, C. Weber, O.A. Yildirim, K. Sotlar, A. Schurmann, S. Zierler, H. Zischka, A.G. Ryazanov, and T. Gudermann. 2016. Epithelial magnesium transport by TRPM6 is essential for prenatal development and adult survival. *Elife*. 5.

Chubanov, V., M. Mederos y Schnitzler, M. Meissner, S. Schafer, K. Abstiens, T. Hofmann, and T. Gudermann. 2012. Natural and synthetic modulators of SK (K(ca)2) potassium channels inhibit magnesium-dependent activity of the kinase-coupled cation channel TRPM7. *Br J Pharmacol*. 166:1357-1376.

Chubanov, V., L. Mittermeier, and T. Gudermann. 2018. Role of kinase-coupled TRP channels in mineral homeostasis. *Pharmacol Ther*. 184:159-176.

de Baaij, J.H., J.G. Hoenderop, and R.J. Bindels. 2015. Magnesium in man: implications for health and disease. *Physiol Rev*. 95:1-46.

Demeuse, P., R. Penner, and A. Fleig. 2006. TRPM7 channel is regulated by magnesium nucleotides via its kinase domain. *J Gen Physiol*. 127:421-434.

Desai, B.N., G. Krapivinsky, B. Navarro, L. Krapivinsky, B.C. Carter, S. Febvay, M. Delling, A. Penumaka, I.S. Ramsey, Y. Manasian, and D.E. Clapham. 2012. Cleavage of TRPM7 releases the kinase domain from the ion channel and regulates its participation in Fas-induced apoptosis. *Dev Cell*. 22:1149-1162.

Duan, J., Z. Li, J. Li, R.E. Hulse, A. Santa-Cruz, W.C. Valinsky, S.A. Abiria, G. Krapivinsky, J. Zhang, and D.E. Clapham. 2018. Structure of the mammalian TRPM7, a magnesium channel required during embryonic development. *Proc Natl Acad Sci U S A*. 115:E8201-E8210.

Fleig, A., and V. Chubanov. 2014. Trpm7. *Handb Exp Pharmacol*. 222:521-546.

Guilbert, A., M. Gautier, I. Dhennin-Duthille, N. Haren, H. Sevestre, and H. Ouadid-Ahidouch. 2009. Evidence that TRPM7 is required for breast cancer cell proliferation. *Am J Physiol Cell Physiol*. 297:C493-502.

Hofmann, T., S. Schafer, M. Linseisen, L. Sytik, T. Gudermann, and V. Chubanov. 2014. Activation of TRPM7 channels by small molecules under physiological conditions. *Pflugers Arch*. 466:2177-2189.

Ilbert, M., P.C. Graf, and U. Jakob. 2006. Zinc center as redox switch--new function for an

old motif. *Antioxid Redox Signal*. 8:835-846.

Inoue, H., M. Inazu, M. Konishi, and U. Yokoyama. 2019. Functional expression of TRPM7 as a Ca(2+) influx pathway in adipocytes. *Physiol Rep*. 7:e14272.

Inoue, H., T. Murayama, M. Tashiro, T. Sakurai, and M. Konishi. 2014. Mg(2+)- and ATP-dependent inhibition of transient receptor potential melastatin 7 by oxidative stress. *Free Radic Biol Med*. 72:257-266.

Inoue, K., D. Branigan, and Z.G. Xiong. 2010. Zinc-induced neurotoxicity mediated by transient receptor potential melastatin 7 channels. *J Biol Chem*. 285:7430-7439.

Jin, J., B.N. Desai, B. Navarro, A. Donovan, N.C. Andrews, and D.E. Clapham. 2008. Deletion of Trpm7 disrupts embryonic development and thymopoiesis without altering Mg2+ homeostasis. *Science*. 322:756-760.

Jin, J., L.J. Wu, J. Jun, X. Cheng, H. Xu, N.C. Andrews, and D.E. Clapham. 2012. The channel kinase, TRPM7, is required for early embryonic development. *Proc Natl Acad Sci U S A*. 109:E225-233.

Kaitsuka, T., C. Katagiri, P. Beesetty, K. Nakamura, S. Hourani, K. Tomizawa, J.A. Kozak, and M. Matsushita. 2014. Inactivation of TRPM7 kinase activity does not impair its channel function in mice. *Sci Rep*. 4:5718.

Kashio, M., T. Sokabe, K. Shintaku, T. Uematsu, N. Fukuta, N. Kobayashi, Y. Mori, and M. Tominaga. 2012. Redox signal-mediated sensitization of transient receptor potential melastatin 2 (TRPM2) to temperature affects macrophage functions. *Proc Natl Acad Sci U S A*. 109:6745-6750.

Klomsiri, C., P.A. Karplus, and L.B. Poole. 2011. Cysteine-based redox switches in enzymes. *Antioxid Redox Signal*. 14:1065-1077.

Krapivinsky, G., L. Krapivinsky, Y. Manasian, and D.E. Clapham. 2014. The TRPM7 chanzyme is cleaved to release a chromatin-modifying kinase. *Cell*. 157:1061-1072.

Krezel, A., and W. Maret. 2016. The biological inorganic chemistry of zinc ions. *Arch Biochem Biophys*. 611:3-19.

Kroncke, K.D., and L.O. Klotz. 2009. Zinc fingers as biologic redox switches? *Antioxid Redox Signal*. 11:1015-1027.

Liu, A., and B. Yang. 2019. Roles of TRPM7 in Renal Ischemia-Reperfusion Injury. *Curr Protein Pept Sci*. 20:777-788.

Liu, H., J.P. Dilger, and J. Lin. 2020. The Role of Transient Receptor Potential Melastatin 7 (TRPM7) in Cell Viability: A Potential Target to Suppress Breast Cancer Cell Cycle. *Cancers (Basel)*. 12.

Liu, W., L.T. Su, D.K. Khadka, C. Mezzacappa, Y. Komiya, A. Sato, R. Habas, and L.W. Runnels. 2011. TRPM7 regulates gastrulation during vertebrate embryogenesis.

Dev Biol. 350:348-357.

Matsushita, M., J.A. Kozak, Y. Shimizu, D.T. McLachlin, H. Yamaguchi, F.Y. Wei, K. Tomizawa, H. Matsui, B.T. Chait, M.D. Cahalan, and A.C. Nairn. 2005. Channel function is dissociated from the intrinsic kinase activity and autophosphorylation of TRPM7/ChaK1. *J Biol Chem.* 280:20793-20803.

Meng, Z., R. Cao, Y. Wang, H. Cao, T. Liu, Z. Yang, and X. Wang. 2014. Suppression of renal TRPM7 may alleviate kidney injury in the renal transplantation. *World J Urol.* 32:1303-1311.

Nadler, M.J., M.C. Hermosura, K. Inabe, A.L. Perraud, Q. Zhu, A.J. Stokes, T. Kurosaki, J.P. Kinet, R. Penner, A.M. Scharenberg, and A. Fleig. 2001. LTRPC7 is a Mg.ATP-regulated divalent cation channel required for cell viability. *Nature.* 411:590-595.

Paravicini, T.M., V. Chubanov, and T. Gudermann. 2012. TRPM7: a unique channel involved in magnesium homeostasis. *Int J Biochem Cell Biol.* 44:1381-1384.

Poole, L.B., and K.J. Nelson. 2008. Discovering mechanisms of signaling-mediated cysteine oxidation. *Curr Opin Chem Biol.* 12:18-24.

Reddie, K.G., and K.S. Carroll. 2008. Expanding the functional diversity of proteins through cysteine oxidation. *Curr Opin Chem Biol.* 12:746-754.

Rhee, S.G., Y.S. Bae, S.R. Lee, and J. Kwon. 2000. Hydrogen peroxide: a key messenger that modulates protein phosphorylation through cysteine oxidation. *Sci STKE.* 2000:pe1.

Romagnani, A., V. Vettore, T. Rezzonico-Jost, S. Hampe, E. Rottoli, W. Nadolni, M. Perotti, M.A. Meier, C. Hermanns, S. Geiger, G. Wennemuth, C. Recordati, M. Matsushita, S. Muehlich, M. Proietti, V. Chubanov, T. Gudermann, F. Grassi, and S. Zierler. 2017. TRPM7 kinase activity is essential for T cell colonization and alloreactivity in the gut. *Nat Commun.* 8:1917.

Romani, A.M. 2011. Cellular magnesium homeostasis. *Arch Biochem Biophys.* 512:1-23.

Runnels, L.W., L. Yue, and D.E. Clapham. 2001. TRP-PLIK, a bifunctional protein with kinase and ion channel activities. *Science.* 291:1043-1047.

Ryazanova, L.V., L.J. Rondon, S. Zierler, Z. Hu, J. Galli, T.P. Yamaguchi, A. Mazur, A. Fleig, and A.G. Ryazanov. 2010. TRPM7 is essential for Mg(2+) homeostasis in mammals. *Nat Commun.* 1:109.

Rybarczyk, P., M. Gautier, F. Hague, I. Dhennin-Duthille, D. Chatelain, J. Kerr-Conte, F. Pattou, J.M. Regimbeau, H. Sevestre, and H. Ouadid-Ahidouch. 2012. Transient receptor potential melastatin-related 7 channel is overexpressed in human pancreatic ductal adenocarcinomas and regulates human pancreatic cancer cell migration. *Int J Cancer.* 131:E851-861.

Schmitz, C., M.V. Dorovkov, X. Zhao, B.J. Davenport, A.G. Ryazanov, and A.L. Perraud. 2005. The channel kinases TRPM6 and TRPM7 are functionally nonredundant. *J Biol Chem*. 280:37763-37771.

Schmitz, C., A.L. Perraud, C.O. Johnson, K. Inabe, M.K. Smith, R. Penner, T. Kurosaki, A. Fleig, and A.M. Scharenberg. 2003. Regulation of vertebrate cellular Mg2+ homeostasis by TRPM7. *Cell*. 114:191-200.

Seneque, O., and J.M. Latour. 2010. Coordination properties of zinc finger peptides revisited: ligand competition studies reveal higher affinities for zinc and cobalt. *J Am Chem Soc*. 132:17760-17774.

Stritt, S., P. Nurden, R. Favier, M. Favier, S. Ferioli, S.K. Gotru, J.M. van Eeuwijk, H. Schulze, A.T. Nurden, M.P. Lambert, E. Turro, S. Burger-Stritt, M. Matsushita, L. Mittermeier, P. Ballerini, S. Zierler, M.A. Laffan, V. Chubanov, T. Gudermann, B. Nieswandt, and A. Braun. 2016. Defects in TRPM7 channel function deregulate thrombopoiesis through altered cellular Mg(2+) homeostasis and cytoskeletal architecture. *Nat Commun*. 7:11097.

Sun, H.S. 2017. Role of TRPM7 in cerebral ischaemia and hypoxia. *J Physiol*. 595:3077-3083.

Sun, H.S., M.F. Jackson, L.J. Martin, K. Jansen, L. Teves, H. Cui, S. Kiyonaka, Y. Mori, M. Jones, J.P. Forder, T.E. Golde, B.A. Orser, J.F. Macdonald, and M. Tymianski. 2009. Suppression of hippocampal TRPM7 protein prevents delayed neuronal death in brain ischemia. *Nat Neurosci*. 12:1300-1307.

Uehara, A., T. Murayama, M. Yasukochi, M. Fill, M. Horie, T. Okamoto, Y. Matsuura, K. Uehara, T. Fujimoto, T. Sakurai, and N. Kurebayashi. 2017. Extensive Ca2+ leak through K4750Q cardiac ryanodine receptors caused by cytosolic and luminal Ca2+ hypersensitivity. *J Gen Physiol*. 149:199-218.

Wolf, F.I., and V. Trapani. 2008. Cell (patho)physiology of magnesium. *Clin Sci (Lond)*. 114:27-35.

Yamaguchi, H., M. Matsushita, A.C. Nairn, and J. Kuriyan. 2001. Crystal structure of the atypical protein kinase domain of a TRP channel with phosphotransferase activity. *Mol Cell*. 7:1047-1057.

Yu, H., Z. Zhang, A. Lis, R. Penner, and A. Fleig. 2013. TRPM7 is regulated by halides through its kinase domain. *Cell Mol Life Sci*. 70:2757-2771.

Zhelay, T., K.B. Wieczerzak, P. Beesetty, G.M. Alter, M. Matsushita, and J.A. Kozak. 2018. Depletion of plasma membrane-associated phosphoinositides mimics inhibition of TRPM7 channels by cytosolic Mg(2+), spermine, and pH. *J Biol Chem*. 293:18151-18167.

Zierler, S., G. Yao, Z. Zhang, W.C. Kuo, P. Porzgen, R. Penner, F.D. Horgen, and A. Fleig. 2011. Waixenicin A inhibits cell proliferation through magnesium-dependent block of transient receptor potential melastatin 7 (TRPM7) channels. *J Biol Chem*. 286:39328-39335.

Figure legends

Figure 1

Mouse TRPM7 is inhibited by oxidative stress induced by H_2O_2 in an $[Mg^{2+}]_i$-dependent manner. (A, B) Effect of H_2O_2 (500 μM) on mTRPM7 current at +80 mV in the presence of 0.2 (A) or 1 mM (B) $[Mg^{2+}]_i$. Under the whole-cell clamp mode, ramp command pulses from -100 to +100 V (1-s duration) were applied every 10 s. Each symbol represents the mean ± SEM (vertical bar) of 10 recordings. (C) $[Mg^{2+}]_i$-dependent inhibition curve of mTRPM7 current under control (black line) and H_2O_2-treated (red line) conditions. Under control conditions, the current was inhibited by intracellular free Mg^{2+} with IC_{50} at 427 μM, whereas, after H_2O_2 treatment, the current was inhibited by intracellular free Mg^{2+} with IC_{50} at 4.3 μM. Each symbol represents the mean ± SEM (vertical bar) of 4-25 observations. (D, E) A Mg^{2+}-insensitive mutant, mTRPM7-S1107E, was not inhibited by H_2O_2 (500 μM) in the presence of 0.2 mM (D) or 1 mM (E) $[Mg^{2+}]_i$. Each symbol represents the mean ± SEM (vertical bar) of 13 recordings. (F) Mean mTRPM7-S1107E current density did not differ in the absence (open bars) or presence (closed bars) of H_2O_2. Each bar represents the mean ± SEM of 6-15 observations. (G) A caspase cleavage-resistant mutant mTRPM7-D1510A was inhibited by H_2O_2 (500 μM) in the presence of 0.2 mM $[Mg^{2+}]_i$. Each symbol represents the mean ± SEM (vertical bar) of six recordings. (H) The inhibitory effect of NMM (100 μM) on mTRPM7 current in the presence of 0.2 mM

$[Mg^{2+}]_i$. Each symbol represents the mean ± SEM (vertical bar) of five recordings. (I) NMM (100 μM) inhibited mTRPM7 current in the presence of 0.2 mM $[Mg^{2+}]_i$ (n = 9) , but not in the absence of intracellular Mg^{2+} (n = 4). Each bar represents the mean ± SEM (vertical bar). *P < 0.05 by paired *t*-test vs. Control.

Figure 2

Screening of cysteines in mTRPM7 responsible for the oxidative stress-induced inhibition. (A) Schematic diagram of 34 cysteines conserved in mouse and human TRPM7. S1107 and D1510 were also depicted (red dots). (B) Expression of TRPM7-wt and its mutants. Immunoblotting of TRPM7 and calnexin (loading control) was carried out with HEK293 cell lysates. Numbers in left represent molecular mass of standards (in kDa). (C) The effect of H_2O_2 on mutant TRPM7 current. Each bar represents the mean ± SEM (vertical bar) of 6-13 observations.

Figure 3

Localization of TRPM7 or its mutants in HEK293 cells. Representative confocal images showing the localization of TRPM7 (green) in doxycycline-untreated (Dox (-)), doxycycline-treated (Dox (+)), mTRPM7-C721A, -C721S, -C738A, -C738S, -C1809S and C1813S-expressing HEK293 cells. Scale bar, 20 μm.

Figure 4

Functional reconstitution of TRPM7 current by co-expression of M7kd in M7cd-expressing cells. (A, B) Doxycycline-treatment induced an increase in current

density (open circles) compared to doxycycline-untreated (open triangles) HEK293 cells transfected with M7cd in the absence of intracellular Mg^{2+} (A), but not in the presence of 0.2 mM $[Mg^{2+}]_i$ (B). Each symbol represents the mean ± SEM (vertical bar) of 8-21 recordings. (C) M7cd-S1107E current density was similar in the absence (open squares) and presence of 0.2 mM $[Mg^{2+}]_i$ (open diamonds). Each symbol represents the mean ± SEM (vertical bar) of 7-10 recordings. (D, E) Transient expression of M7kd in M7cd-expressing cells resulted in an increase in M7cd current density that was inhibited by H_2O_2 (500 μM) in the presence of 0.2 mM $[Mg^{2+}]_i$ (D), but not in the absence of intracellular Mg^{2+} (E). Each symbol represents the mean ± SEM (vertical bar) of eight recordings. (F) $[Mg^{2+}]_i$-dependent inhibition curves of M7cd with (red line) or without (blue line) co-expression of M7kd. The current in HEK293 cells expressing M7cd alone was inhibited by intracellular free Mg^{2+} with IC_{50} at 5.6 μM. Co-expression of M7kd attenuated the inhibition by intracellular Mg^{2+} with IC_{50} at 4.3 μM. Each symbol represents the mean ± SEM (vertical bar) of 5-28 observations. (G) The time course of mM7cd current when M7kd was transfected by either lipofection (closed circles) or baculovirus infection (open squares) in the presence of 0.2 mM $[Mg^{2+}]_i$. Each symbol represents the mean ± SEM (vertical bar) of 8-20 observations. (H) The effect of H_2O_2 (500 μM) on M7cd current in the presence of 0.2 mM $[Mg^{2+}]_i$ in cells transfected with M7kd by baculovirus infection. Each symbol represents the mean ± SEM (vertical bar) of four recordings. (I) Co-expression of M7kd by either lipofection or baculovirus infection similarly exhibited the current sensitive to H_2O_2 (500 μM) in M7cd-expressing HEK293 cells. Each bar represents the mean ± SEM (vertical bar) of eight (lipofectamine 3000) or four observations (baculovirus). *$P < 0.05$ vs. Control. (J) The effect of co-expression with kinase-inactive mutant M7kd-1645R on M7cd current.

Each symbol represents the mean ± SEM (vertical bar) of four recordings. (K) The effect of TRPM6 kinase domain (M6kd) co-expression on M7cd current. Each symbol represents the mean ± SEM (vertical bar) of eight recordings.

Figure 5

Mutation in the zinc-binding motif in M7kd disrupts the interaction between M7cd and M7kd to attenuate $[Mg^{2+}]_i$-dependent inhibition of the M7cd current. (A) Separate protein expression of M7cd and M7kd in M7cd-expressing HEK293 cells transfected with M7kd-wt (lane 2), M7kd-C1809S (lane 3), M7kd-C1813S (lane 4), H1751A (lane 5), or H1808A (lane 6). M7cd expression (172 kDa, arrow) is induced by doxycycline treatment. M7kd expression (40 kDa, arrowhead) is induced by baculovirus infection. (B-C) The effect of M7kd-C1809S (B) or -C1813S (C) expression on M7cd current induced by lipofection. Each symbol represents the mean ± SEM of 8-12 recordings. (D) Expression of M7kd-C1809S does not affect M7cd-S1107E current. Each symbol represents the mean ± SEM of six recordings. (E, F) The effect of M7kd-H1750A (E) or -H1807A (F) expression on M7cd current. Each symbol represents the mean ± SEM of 7-8 recordings. (G) M7 current densities at 2 min after break-in in M7kd-wt (WT), -C1809S, -C1813S, -H1750A, or –H1807A-coexpressing cells.

Figure 6

Schematic illustration of TRPM7 regulation by oxidative stress.

Supplemental Figure

The effect of oxidative stress induced by H_2O_2 on human TRPM7 current. (A, B) A representative trace of whole-cell currents showing the time course of the current inhibition by H_2O_2 (500 μM) in the presence (A) or absence (B) of 0.2 mM $[Mg^{2+}]_i$ in a human TRPM7 (hTRPM7)-expressing HEK293 cell. (C) H_2O_2 (500 μM) inhibited hTRPM7 current in the presence of 0.2 mM $[Mg^{2+}]_i$ (n = 6), but not in the absence of intracellular Mg^{2+} (n = 5). Each bar represents the mean ± SEM (vertical bar). *P < 0.05 vs. Control. (D) NMM (100 μM) inhibited hTRPM7 current in the presence of 0.2 mM $[Mg^{2+}]_i$ (n = 5) , but not in the absence of intracellular Mg^{2+} (n = 4). Each bar represents the mean ± SEM (vertical bar). *P < 0.05 vs. Control.

Figure 1

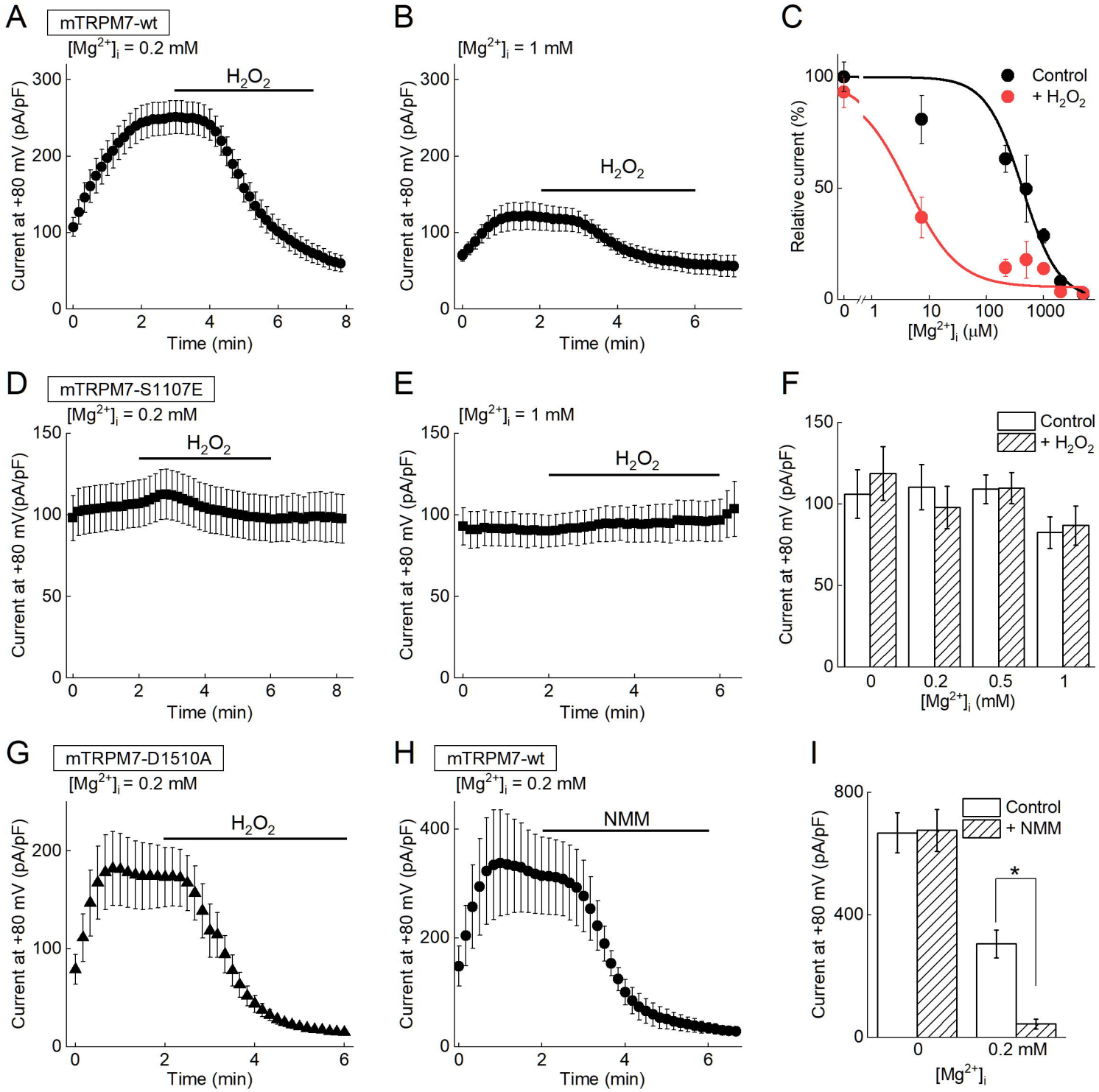
A
mTRPM7-wt
[Mg2+]i = 0.2 mM
H2O2
Current at +80 mV (pA/pF)
Time (min)
B
[Mg2+]i = 1 mM
H2O2
Current at +80 mV (pA/pF)
Time (min)
C
Control
+ H2O2
Relative current (%)
[Mg2+]i (μM)
D
mTRPM7-S1107E
[Mg2+]i = 0.2 mM
H2O2
Current at +80 mV(pA/pF)
Time (min)
E
[Mg2+]i = 1 mM
H2O2
Current at +80 mV (pA/pF)
Time (min)
F
Control
+ H2O2
Current at +80 mV (pA/pF)
[Mg2+]i (mM)
G
mTRPM7-D1510A
[Mg2+]i = 0.2 mM
H2O2
Current at +80 mV (pA/pF)
Time (min)
H
mTRPM7-wt
[Mg2+]i = 0.2 mM
NMM
Current at +80 mV (pA/pF)
Time (min)
I
Control
+ NMM
Current at +80 mV (pA/pF)
0.2 mM
[Mg2+]i

Figure 2

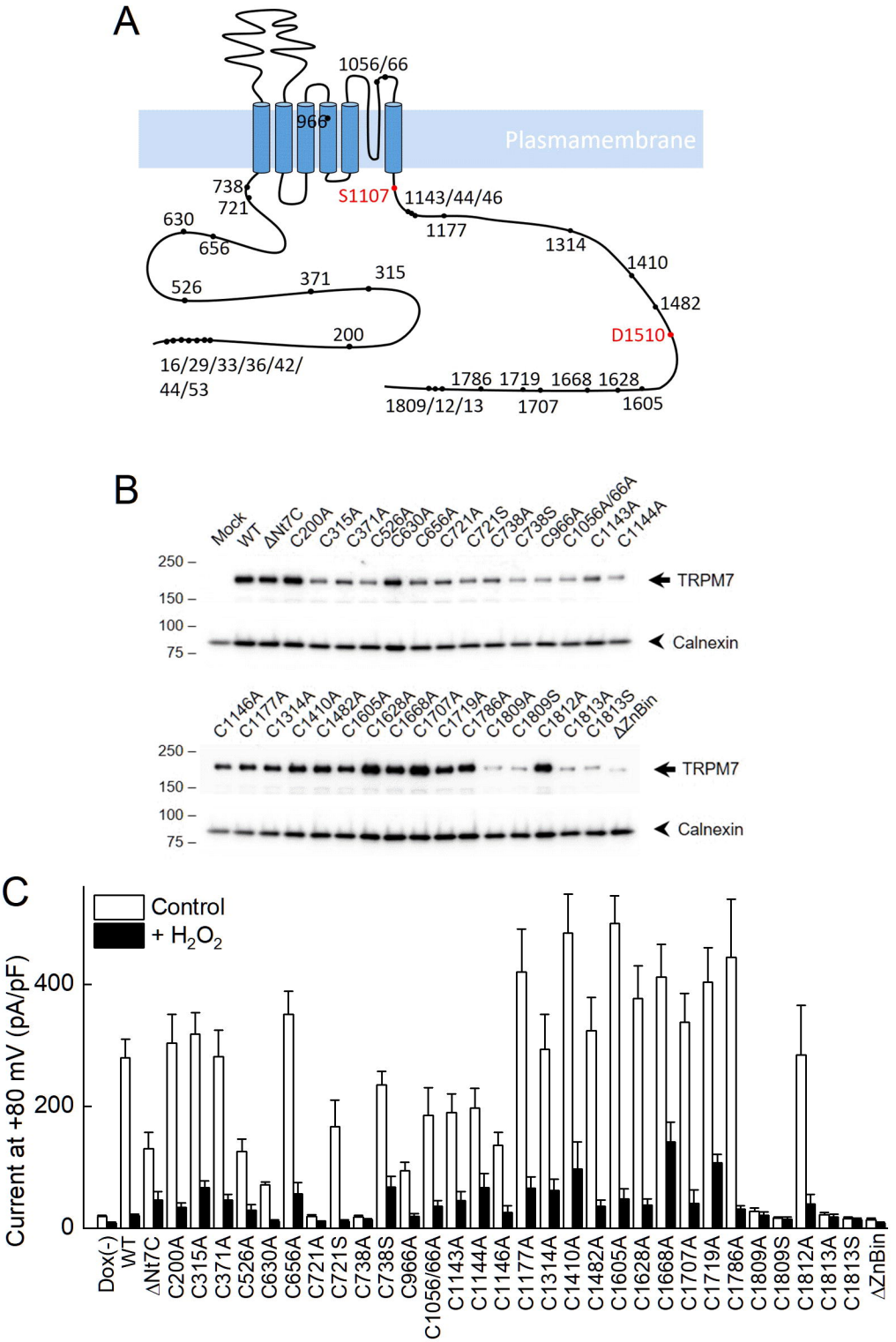
A
Plasmamembrane
1056/66
966
738
721
S1107
1143/44/46
630
656
1177
1314
1410
526
371
315
1482
200
D1510
16/29/33/36/42/
44/53
1786 1719 1668 1628
1809/12/13
1707
1605
B
Mock
WT
ΔNt7C
C200A
C315A
C371A
C526A
C630A
C656A
C721A
C721S
C738A
C738S
C966A
C1056A/66A
C1143A
C1144A
250 –
150 –
100 –
75 –
TRPM7
Calnexin
C1146A
C1177A
C1314A
C1410A
C1482A
C1605A
C1628A
C1668A
C1707A
C1719A
C1786A
C1809A
C1809S
C1812A
C1813A
C1813S
ΔZnBin
250 –
150 –
100 –
75 –
TRPM7
Calnexin
C
Control
+ H2O2
Current at +80 mV (pA/pF)
400
200
0
Dox(-)
WT
ΔNt7C
C200A
C315A
C371A
C526A
C630A
C656A
C721A
C721S
C738A
C738S
C966A
C1056/66A
C1143A
C1144A
C1146A
C1177A
C1314A
C1410A
C1482A
C1605A
C1628A
C1668A
C1707A
C1719A
C1786A
C1809A
C1809S
C1812A
C1813A
C1813S
ΔZnBin

Figure 3

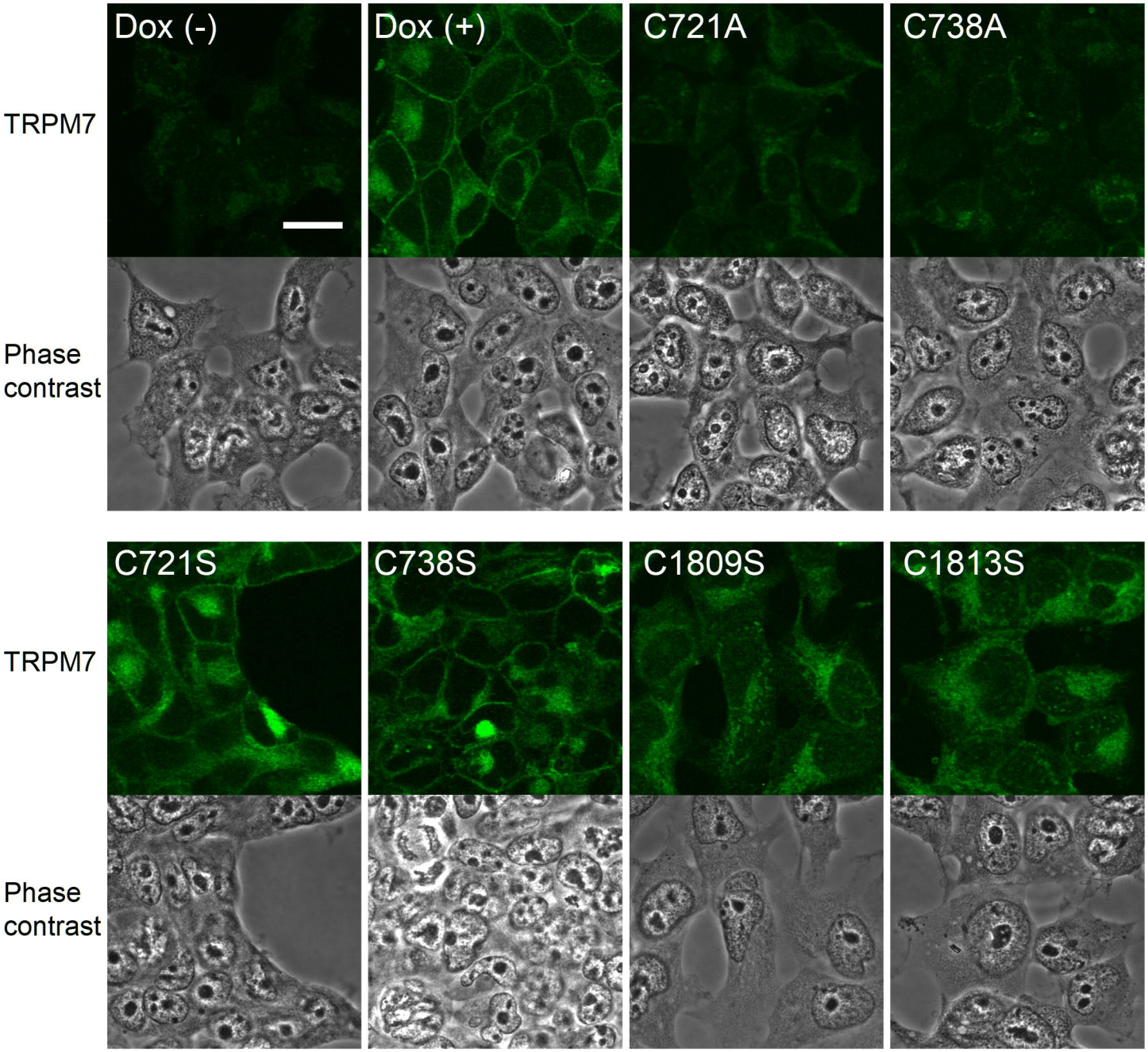
Dox (-)
Dox (+)
C721A
C738A
TRPM7
Phase contrast
C721S
C738S
C1809S
C1813S
TRPM7
Phase contrast

Figure 4

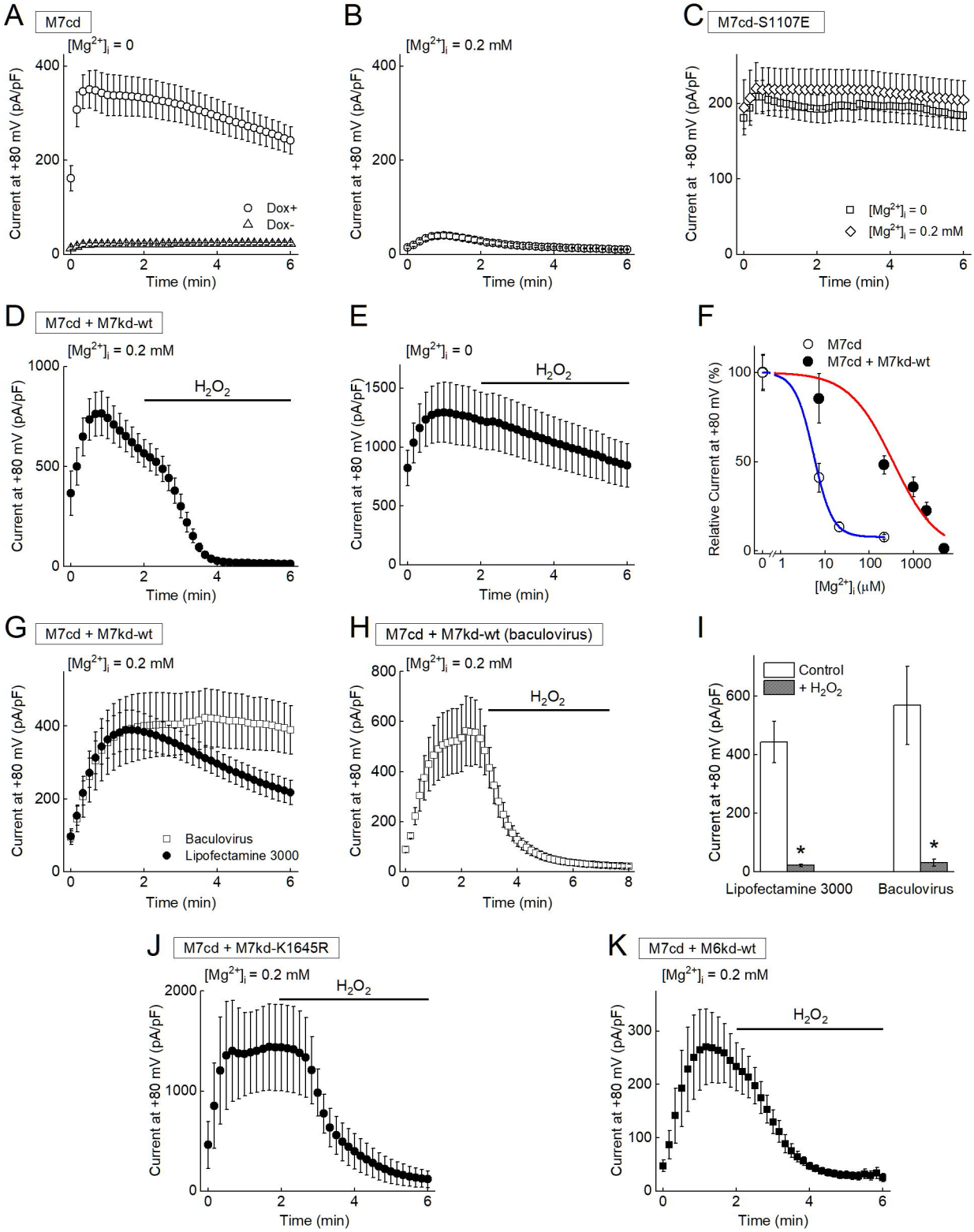
A
M7cd
[Mg2+]i = 0
Current at +80 mV (pA/pF)
Time (min)
Dox+
Dox-
B
[Mg2+]i = 0.2 mM
C
M7cd-S1107E
[Mg2+]i = 0
[Mg2+]i = 0.2 mM
D
M7cd + M7kd-wt
[Mg2+]i = 0.2 mM
H2O2
E
[Mg2+]i = 0
F
M7cd
M7cd + M7kd-wt
Relative Current at +80 mV (%)
[Mg2+]i (μM)
G
M7cd + M7kd-wt
[Mg2+]i = 0.2 mM
Baculovirus
Lipofectamine 3000
H
M7cd + M7kd-wt (baculovirus)
[Mg2+]i = 0.2 mM
H2O2
I
Control
+ H2O2
Lipofectamine 3000
Baculovirus
J
M7cd + M7kd-K1645R
[Mg2+]i = 0.2 mM
H2O2
K
M7cd + M6kd-wt
[Mg2+]i = 0.2 mM
H2O2

Figure 5

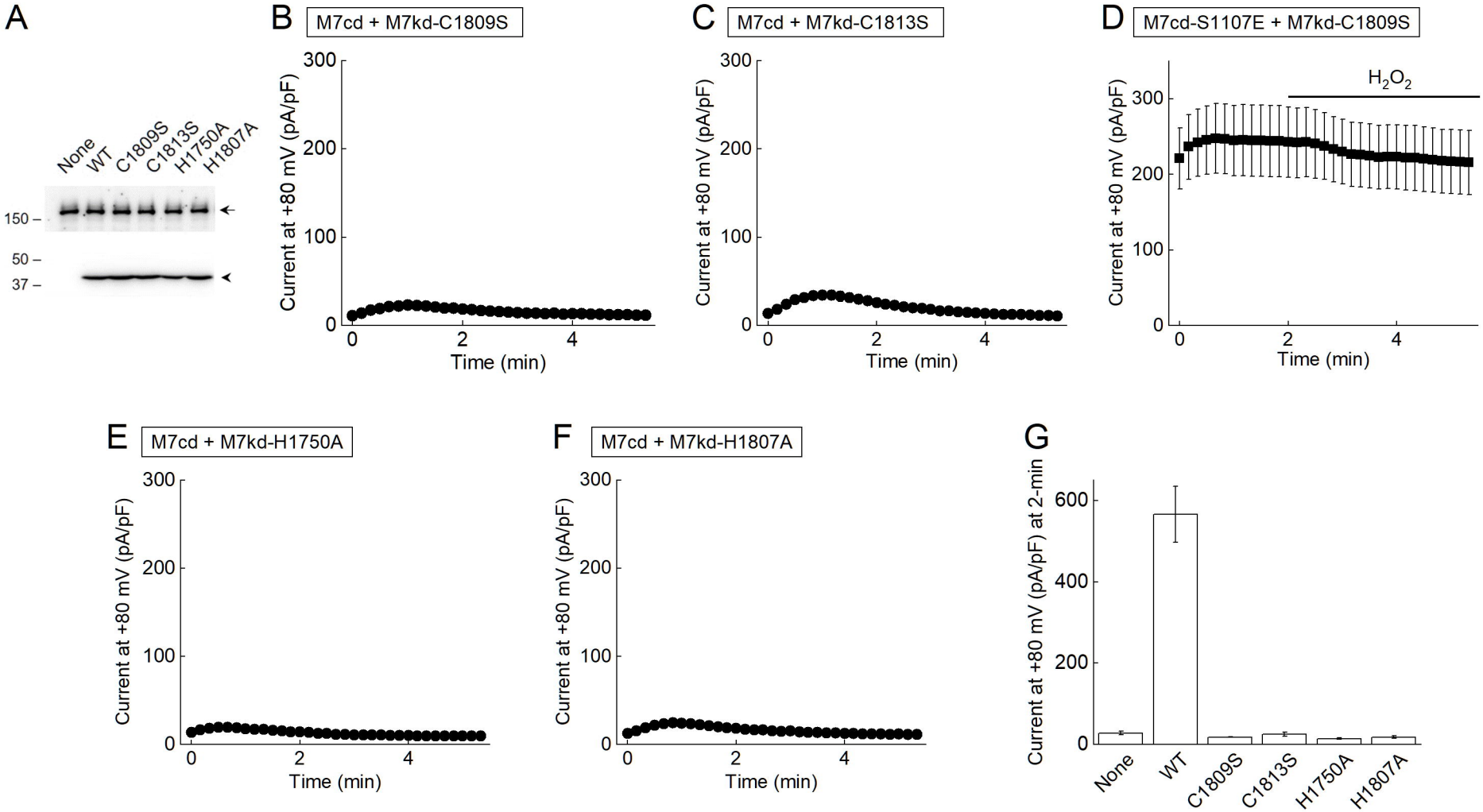
A
None
WT
C1809S
C1813S
H1750A
H1807A
150 –
50 –
37 –
B
M7cd + M7kd-C1809S
C
M7cd + M7kd-C1813S
D
M7cd-S1107E + M7kd-C1809S
H_2O_2
Current at +80 mV (pA/pF)
Time (min)
E
M7cd + M7kd-H1750A
F
M7cd + M7kd-H1807A
G
Current at +80 mV (pA/pF) at 2-min

Figure 6

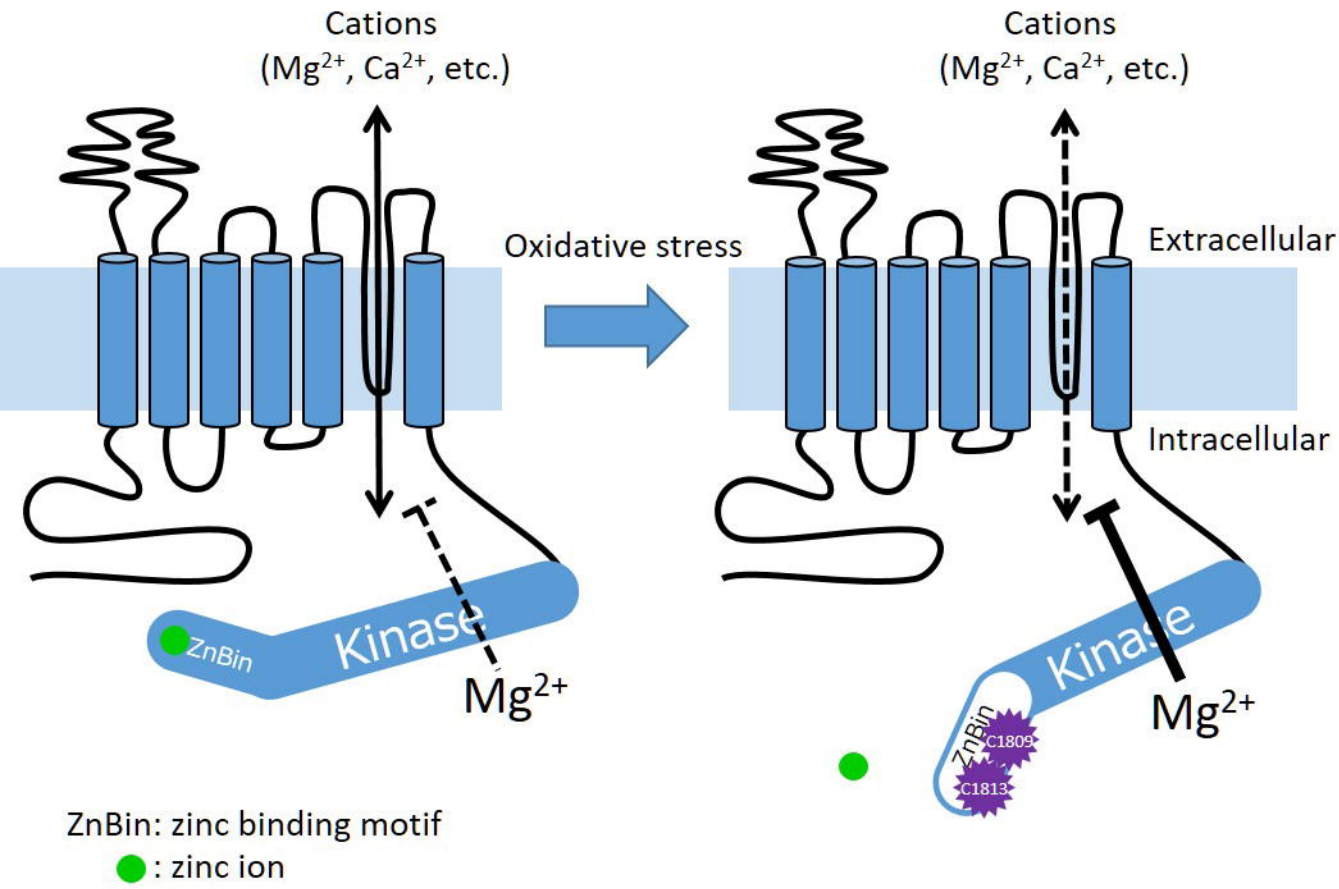
Cations
(Mg^{2+}, Ca^{2+}, etc.)
Oxidative stress
Cations
(Mg^{2+}, Ca^{2+}, etc.)
Extracellular
Intracellular
ZnBin
Kinase
Mg^{2+}
ZnBin
Kinase
C1809
C1813
Mg^{2+}
ZnBin: zinc binding motif
: zinc ion